# Matrix deformations around angiogenic sprouts correlate to sprout dynamics and suggest pulling activity*

**Marie-Mo Vaeyens[1], Alvaro Jorge-Peñas[1], Jorge Barrasa-Fano[1], Christian Steuwe[2], Tommy Heck[1], Peter Carmeliet[3,4], Maarten Roeffaers[2], and Hans Van Oosterwyck[1,5,@]**

[1] Biomechanics Section (BMe), Department of Mechanical Engineering, KU Leuven, Leuven, Belgium;
[2] Centre for Membrane Separations, Adsorption, Catalysis and Spectroscopy for Sustainable Solutions (cMACS), Department of Microbial and Molecular Systems (M²S), KU Leuven, Leuven, Belgium;
[3] Laboratory of Angiogenesis and Vascular Metabolism, VIB Center for Cancer Biology (CCB), VIB, Leuven, Belgium;
[4] Laboratory of Angiogenesis and Vascular Metabolism, Department of Oncology and Leuven Cancer Institute (LKI), KU Leuven, Leuven, Belgium;
[5] Prometheus, div. Skeletal Tissue Engineering, KU Leuven, Leuven, Belgium;
[@] Correspondence should be addressed to Hans Van Oosterwyck (Hans.VanOosterwyck@kuleuven.be).

**ACKNOWLEDGMENTS**: The authors are grateful for funding support from the Research Foundation Flanders (FWO) (doctoral fellowship to T.H., postdoctoral fellowship to C.S., FWO grants G.0821.13, G0B9615N, G087018N), from the Hercules-foundation (G0H6316N), from KU Leuven internal funding (C14/17/111) and from the European Research Council under the European Union's Seventh Framework Program (FP7/2007-2013)/ ERC Grant Agreement n°308223) to H.V.O. We are grateful to Anna Rita Cantelmo, Sandra Schoors, Inge Betz and Joris Souffreau for cell culture tips and techniques. We thank Evan Claes and Tobie Martens for their contributions to the experimental microscopy set-up and the live imaging.

**KEYWORDS**: sprouting angiogenesis, *in vitro* model, endothelial invasion, extracellular matrix, collagen, cytoskeleton, mechanobiology, mechanotransduction, cellular forces, pulling forces, computer model, image processing, confocal microscopy

**Angiogenesis is the formation of new blood vessels from the pre-existing vasculature. It is essential for normal tissue growth and regeneration, but also plays a key role in many diseases [1]. Cytoskeletal components have been shown to be important for angiogenic sprout initiation and maintenance [2] as well as endothelial cell shape control during invasion [3]. The exact nature of cytoskeleton-mediated forces for sprout initiation and progression, however, remains poorly understood. Questions on the importance of tip cell pulling versus stalk cell pushing are to a large extent unanswered, which among others has to do with the difficulty of quantifying and resolving those forces in time and space. We developed methods based on time lapse confocal microscopy and image processing – further termed 4D displacement microscopy - to acquire detailed, spatially and temporally resolved extracellular matrix (ECM) deformations, indicative of cell-ECM mechanical interactions around invading sprouts. We demonstrate that matrix deformations dependent on actin-mediated force generation are spatio-temporally correlated with sprout morphological dynamics. Furthermore, sprout tips were found to exert radially pulling forces on the extracellular matrix, which were quantified by means of a computational model of collagen ECM mechanics. Protrusions from extending sprouts mostly increase their pulling forces, while retracting protrusions mainly reduce their pulling forces. Displacement microscopy analysis further unveiled a characteristic dipole-like deformation pattern along the sprout direction that was consistent among seemingly very different sprout shapes - with oppositely oriented displacements at sprout tip versus sprout base and a transition zone of negligible displacements in between. These results demonstrate that sprout-ECM interactions are dominated by pulling forces and underline the key role of tip cell pulling for sprouting angiogenesis.**

* "This is a post-peer-review, pre-copyedit version of an article accepted for publication in *Angiogenesis*. The final authenticated version will be available online at: https://doi.org/10.1007/s10456-020-09708-y"

Angiogenic sprouts are known to be highly dynamic multicellular entities. Different mechanisms are contributing to sprout elongation, such as cell positional rearrangements, (stalk) cell elongation and division. While tip cell pulling on stalk cells, stalk cell pushing on tip cells, or both, have previously been postulated as mechanical forces that underlie sprout elongation [4–10], forces during sprout progression have never been measured, so that the nature and role of physical forces during sprout elongation remain unclear. While the measurement of cell-cell forces is far from trivial, cell-ECM forces can be quantified by means of Traction Force Microscopy (TFM). TFM computes cellular tractions from the measurement of cell-induced ECM deformations by solving the equations that govern ECM mechanical behaviour, provided ECM mechanical properties are known. Reinhart-King and co-workers for example applied TFM measurements to demonstrate a correlation between cellular tractions and the metastatic potential over several cell lines [11] and to investigate the complex interplay between substrate mechanics and endothelial cell behavior [12, 13]. Even if tractions cannot be recovered (e.g. in the absence of any information on ECM mechanical properties), the measurement of ECM deformations (and calculation of deformation-based metrics) can provide quantitative information on cell-ECM mechanical interactions [14]. This is especially true if all measurements are done in the same ECM material, such as is the case in our study. There is a growing body of evidence regarding the importance of acto-myosin based cellular tractions for sprout initiation, dynamics and maintenance [2, 3, 15, 16]. While traction forces around sprouts have not been reported, a limited number of reports exist on ECM deformations around angiogenic sprouts [16–19]. More specifically, Du *et al.* indicated a link between changes in sprout morphology and gel displacements as well as characteristic displacement patterns around tip and stalk cells and in the vicinity of protruding and retracting lamellipodia [17, 19]. In line with these results, Kniazeva *et al.* found a correlation between the overall extent of capillary sprouting and the rate of matrix deformation [18]. While both groups provide evidence for ECM motion between consecutive time points of time lapse experiments as a result of sprout tip motion, none of the studies have attempted to calculate ECM displacements with respect to an undeformed, stress-free ECM state. The latter is required to unambiguously judge on the pulling versus pushing nature of cellular forces. In a 3D TFM experiment, this is typically done by adding a chemical compound at the end of the experiment that disrupts a cell's cytoskeleton, so that the ECM relaxes to its undeformed state [20–25]. One should realize that only elastic ECM deformations can be recovered in this way, while inelastic (plastic) ECM deformations are permanent (irreversible) and therefore remain

unresolved [26, 27]. More recently, Yoon *et al.* were the first to our knowledge to report ECM displacements with respect to an ECM stress-free state – further termed absolute displacements - around in vitro angiogenic sprouts. They observed significant deformations generated at the sprout tips, and less near the stalk cells, which is also coherent with the fan-like collagen fiber pattern at the sprout tips reported by the Utzinger Lab [28], and with data from 3D embedded single cells pulling at long slender extensions [29]. While the qualitative assessment from Yoon *et al.* based on a stress-free state more strongly confirms some of the patterns observed (without a stress-free reference state) around tip and stalk cells by Du *et al.* [17], we consolidate their qualitative observations by providing a spatio-temporal statistical analysis of displacement field patterns and sprout morphology to assess the pulling versus pushing nature of forces underlying short-term (order of one hour) sprout protrusion dynamics during endothelial invasion and sprouting. We next take this displacement microscopy analysis a step further, by reporting for the first time cellular traction forces around in vitro angiogenic sprouts, calculated with a computational model.

We first adapted a 3D *in vitro* model of endothelial sprouting [30] to enable time-lapse confocal microscopy-based quantification of 3D cell-induced matrix displacements around angiogenic sprouts**)**. Fluorescent nanobeads (200 nm diameter) were embedded into a collagen matrix (hydrogel), which served as fiducial markers for matrix displacement calculations**.** In house 4D displacement microscopy algorithms, based on Free Form Deformation (FFD)-based non-rigid image registration [24] were applied for displacement calculation. An overview of the experimental and computational workflow is given in Fig. 1, and extended in Supplementary Fig. S1. Positional stability of the setup was verified by means of spatio-temporal image correlation spectroscopy (STICS) on acellular hydrogel samples to rule out any spurious displacements not related to cellular activity **(Supplementary Fig. S2)**. In order to obtain a stress-free reference state of the hydrogel, Cytochalasin D (CytoD), an inhibitor of actin polymerization, was selected as force relaxing agent [20, 22–25]. Imaging chamber geometry was adapted to ensure proper diffusion of CytoD through the chamber **(Supplementary Fig. S3)**. Sprouts in this study were examined for specific time periods while sprouting in endothelial cell growth medium (EGM2), in DMSO (the solvent of CytoD), during gradual force relaxation (60 min of 500 nM CytoD) or during more rapid relaxation (60 min of 4 µM CytoD). Sprouts from all conditions were subjected to the more rapid relaxation treatment – further referred to as relaxation – during the last

hour of the time lapses in order to retrieve a stress-free state. Rapid relaxation was consistently initiated at t = 90 min and lasted for 60 minutes, except for control experiments with extended durations (in which case 4 µM of CytoD was added for 90 minutes instead of 60 minutes; see representative sprout shown in **Supplementary Fig. S4**). At a concentration of 4 µM CytoD was found to robustly relax matrix displacements within 60 min to a basal level **(Supplementary Fig. S1i** and **Supplementary Fig. S4)** without disrupting overall sprout morphology **(Supplementary Fig. S1c, d** and **Supplementary Video 1)**.

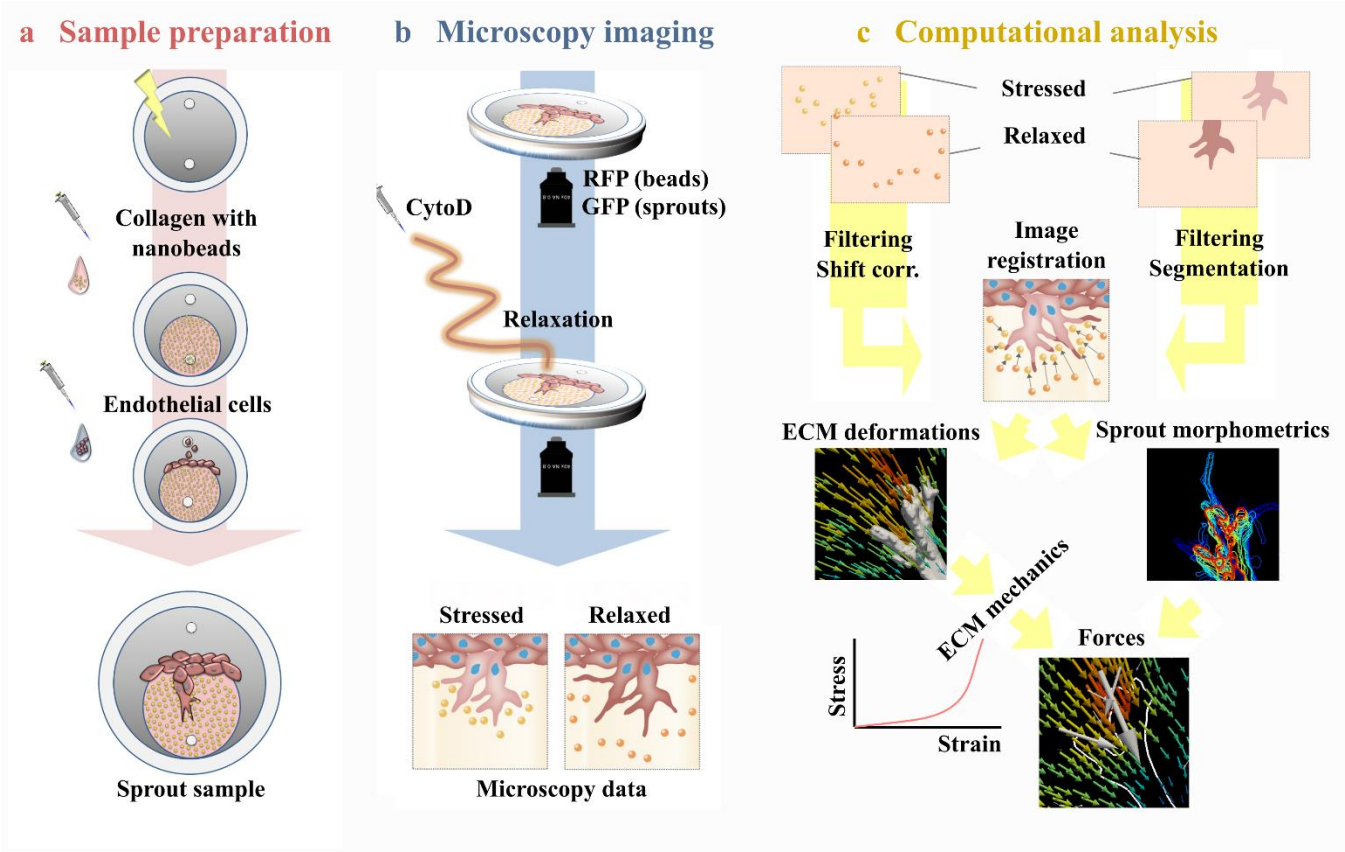


**Fig. 1** Workflow of 4D displacement microscopy around *in vitro* angiogenic sprouts. **(a)** Sample preparation. Imaging chambers are sterilized with UV light. Collagen with nanobeads is introduced in one inlet of the chamber. Endothelial cells are seeded on the polymerized collagen through the other inlet. After cell attachment, cells invade the collagen and form endothelial sprouts. See Supplementary Fig. S1 for a photograph of an imaging chamber and a representative image of the formed sprouts. **(b)** Microscopy imaging. Samples are imaged with confocal laser microscopy for visualization of beads (RFP) and sprouts (GFP). Cytochalasin D is added through a securely fastened tube to relax the system and obtain a stress-free reference state. See Supplementary Fig. S1 for microscopy images of a representative sprout during these steps. **(c)** Computational analysis. The microscopy data is filtered and shift-corrected. Sprouts are segmented and sprout morphometrics quantified. Deformation metrics are calculated based on image registration algorithms. A computational model using extracellular matrix (ECM) mechanical properties is used to calculate forces from the matrix deformations. Each of the steps from the workflow is elaborated in the Methods section within the Supplementary Information

To examine how sprout morphology **(**and its change with time, **Fig. 2a,e)** is correlated to matrix displacement fields **(Fig. 2b,f)**, we defined a number of sprout morphometric readouts **(**sprout length, surface area, volume and solidity; see **Methods** and **Supplementary Fig. S5)**, and additionally assigned the sprouts to subgroups with either multiple end protrusions **(Fig. 2a-d)** or single end protrusions **(Fig. 2e-h)**. Mean and total displacement metrics were defined in order to characterize the mean and total cell-matrix mechanical activity respectively within a 5 µm region around the sprout surface. Apart from calculating these metrics for absolute displacements, we also looked at displacement field dynamics, by comparing bead positions at a given time point with the positions at the previous time point (see **Methods**). These so called incremental displacement fields (for a time increment equal to the scan interval $\tau = 5$ min) are indicative of changes of cell mechanical activity (dynamics) with time (**Fig. 2d,h**). While Kniazeva *et al.* reported a correlation between the overall extent of capillary sprouting and the rate of matrix deformation [18], surprisingly, we found that none of the sprout shape descriptors were correlated to the matrix displacement metrics, suggesting that differences in sprout mechanical activity (intensity and dynamics) between sprouts cannot be explained from morphological differences between sprouts **(**see **Fig. 2i** for sprout volume versus total absolute displacement and **Supplementary Table 1** for all correlations**)**. However, when analyzing changes in sprout volume between consecutive time points **(Fig. 2c,g, Methods** and **Supplementary Fig. S5),** a high correlation was found between changes in sprout volume and the total incremental matrix displacements (**Fig. 2j** and **Supplementary Table 1)**. This suggests a strong link between sprout morphological dynamics and matrix displacement dynamics (and underlying cell-matrix mechanical activity); a link previously proposed by Du *et al.* [17, 19]. Note the colored ovals grouping data points in Figs. 2i and 2j, which highlight the correlation present in 2j and absent in 2i. Further inspection of the sprout subgroups revealed that sprouts with multiple end protrusions displayed significantly higher volumetric changes **(Fig. 2k**, $p = 0.0061$**)** and (in line with the above correlation) also more associated incremental matrix displacements **(Fig. 2l**, $p = 0.0289$**)**. This observation was further substantiated by the fact that sprouts with a lower solidity (**Supplementary Fig. S5**) and thus more (main and/or minor) protrusions showed marginally more total incremental displacements ($p = 0.0462$). Given the fact that the presence of these protrusions can be associated to higher sprout dynamics dynamics (which could also explain the correlation found by Kniazeva *et al.* between a total network length and deformations), we conclude from our statistical analysis that sprout dynamics rather than

sprout morphology is tightly linked to matrix displacement dynamics, which in turn is governed by the dynamics of cell mechanical activity.

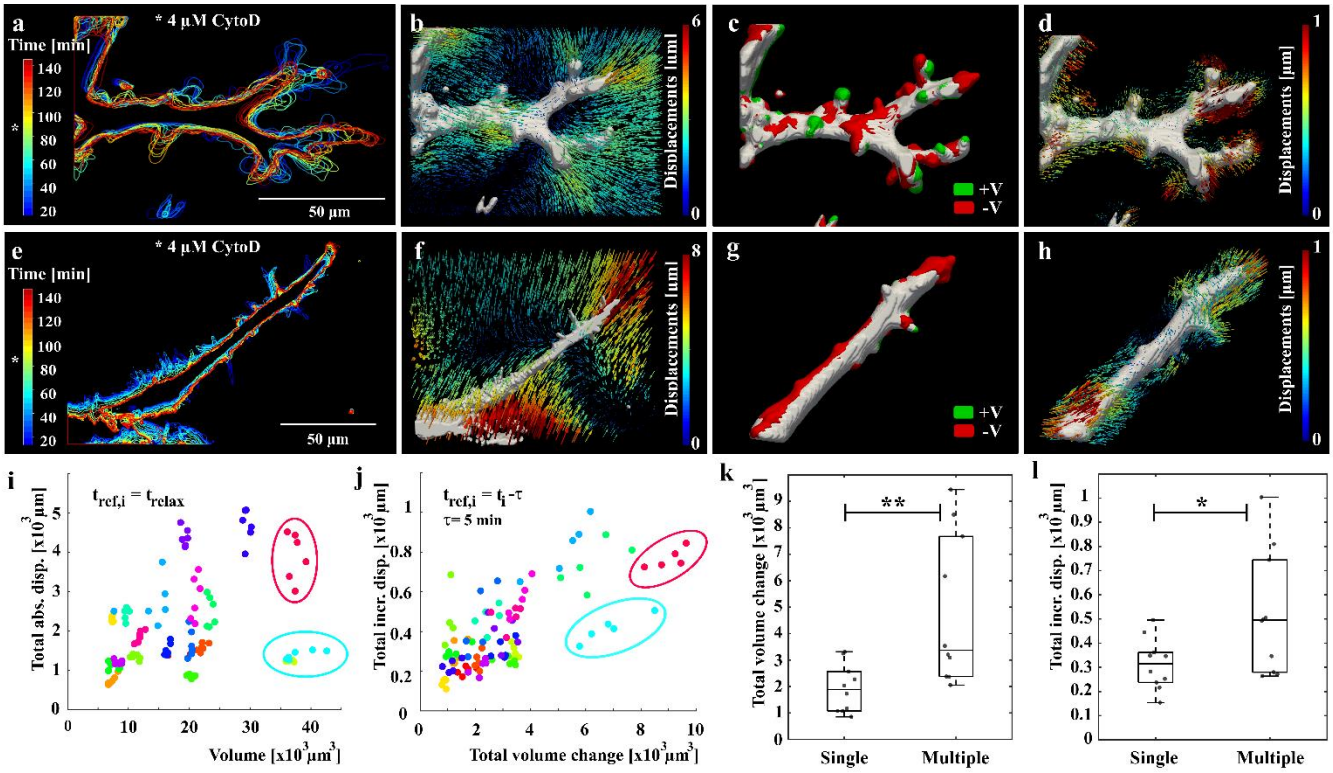


**Fig. 2** Sprout morphological dynamics correlate to matrix displacement dynamics. **(a,e)** Sprout contour evolution plots with time (zt-projection) of representative in vitro angiogenic sprouts with multiple (a) or a single end protrusion(s) (e), being relaxed with 4 µM Cyto added at t = 90 min. Apart from panels (a) and (e) all panels of the figure represent data from the sprouts in growth medium. **(b,f)** Absolute displacements around the sprouts in (a) and (e) for a randomly selected analysed time point in medium before relaxation (0 – 25 min). **(c,g)** Volume changes between 2 consecutive time points before relaxation (interval $\tau$ = 5 min) of the sprouts represented in (a) and (e). Green = increase of sprout volume and red = decrease of sprout volume. **(d,h)** Incremental displacements shown for a 5 µm region around the sprout surface between the same 2 consecutive time points before relaxation as in (c) and (g). **(i)** Sprout volume versus total absolute matrix displacements. Data set of 20 sprouts, with 6 time points (0 – 25 min) before relaxation analysed per sprout (circles with same color, further highlighted for two sprouts by means of ovals). **(j)** Total change in sprout volume versus total incremental displacements (interval $\tau$ = 5 min). Data set of 20 sprouts, with 6 time points (0 – 25 min) before relaxation analysed per sprout (circles with same color). **(k)** Boxplot of total change in sprout volume between 2 consecutive time (interval $\tau$ = 5 min) for sprouts with single or multiple end protrusion(s). **(l)** Boxplot of total incremental displacements for the sprouts in (k) with single or multiple end protrusions. Boxplots are based on a data set of 10 sprouts with a single and 10 sprouts with multiple end protrusions, for a single (randomly selected) time point before sprout relaxation was induced. Displacement metrics were calculated for matrix displacements within a 5 µm region around the sprout surface. See Methods for details on displacement and morphological metrics respectively. Significant p-values are indicated with * for $p < 0.05$ and ** for $p < 0.01$ (see Supplementary Table 2)

When analyzing the distribution of absolute displacements, a characteristic pattern could be observed that was consistent over different sprout shapes (**Fig. 3a**). In this study, sprout tips were defined as the extremities of the sprout branches and sprout bases as the intersection between the sprout and the cell layer. Absolute displacements peaked around sprout tips and were radially oriented towards the tips, indicative of cellular pulling forces from the

sprout protrusions. Less frequently, some clusters of absolute displacements near the tip were found oriented away from the tip, indicative of pushing forces (see **Supplementary Fig. S6**). Elevated displacements were also found close to the sprout base (that is connected to the cell layer on the collagen hydrogel), however their orientation was more variable. For the majority of the sprouts (12 out of a data set of 20 sprouts) absolute displacements at the base were oriented opposite to the displacements at the tip, i.e. pointing towards the tip (similar to the sprout shown in **Fig. 3a**).

This inward movement (i.e. from the cell layer towards the sprout tip) at the base could be the result of pulling forces from the sprout base, pushing forces from the nearby cellular layer or both. In between the sprout and base, there is a zone – that we called zone of convergence – where absolute displacements are close to zero and change sign when moving from base to sprout.

Matrix displacement patterns were also found to remain relatively stable with time during (gradual) relaxation. While absolute displacement values diminished with time due to force relaxation and while the sprout became less dynamic (loss of protrusions**)**, the characteristic dipole-like displacement pattern (pulling pattern) remained (**Supplementary Video 2).** Incremental displacement fields after CytoD application were also calculated and clearly showed matrix unloading (matrix moving away from the sprout) around individual protrusions due to diminishing pulling forces at the sprout tips **(Fig. 3b,c)**. Note how matrix unloading is taking place around one of the protrusions (**Fig. 3b** and later **Fig. 3c** ) while absolute displacements from the corresponding time points (**Fig. 3d** and later **Fig. 3e**) show sustained matrix deformations towards the protrusion. For comparison, legends in Figs 3b-e are set to the same maximal value of 2 µm. See Supplementary Video 2 for absolute displacement values > 2 µm.

In order to better appreciate whether matrix deformation around the sprout was mainly tensile or compressive, we calculated the principal strain components (of the Green-Lagrange strain tensor, which can be derived from the gradient of the absolute displacement field; see **Methods**). We then plotted the major principal strain component,

i.e. the principal component with the largest absolute value, which by convention has a negative sign in case of compression (in which case it is equal to the minimum principal strain) and a positive sign in case of tension (in which case it is equal to the maximum principal strain) (**Fig. 3f**). One notices that compressive strains are dominant for the majority of the matrix around the sprout. Near the sprout stalk, compressive principal strains are more or less parallel to the sprout surface, which is in line with the fact that the mechanical activity of the selected sprout resembles that of a force dipole (and the matrix in between the force poles therefore becomes compressed). Compressive strains are relatively high and can reach values down to several tens of percent. Even in front of the sprout tips, compressive strains dominate, despite the fact that these tips pull on the surrounding matrix (**Fig. 3f** and **Supplementary Fig. S7a-b**). When zooming in on one of these sprout tips, maximum (i.e. tensile) principal strains are found in radial directions with respect to the sprout tip (in line with radially pulling forces) **(Fig. 3g,** right**)**, while minimum (i.e. compressive) principal strains are perpendicular to those directions **(Fig. 3g,** left**)**. The fact that absolute values of compressive strains are higher than those of tensile strains in matrix areas that are loaded in tension, can be explained if the Poisson's ratio of the collagen, when loaded in tension, is larger than one (i.e. lateral shrinkage is larger than applied extension). Such high values have indeed been reported for collagen under tension by Steinwachs *et al.* [20].

We developed a computational model of the mechanical behaviour of the collagen matrix surrounding a selected sprout to identify the cellular forces that were responsible for the observed displacements for that particular sprout (see **Supplementary Fig. S8** and **Methods**). The computational model (limited to a 2D section) could match the characteristic displacement distribution and magnitudes for a cellular force distribution around the sprout (**Fig. 3h**) that resembles to some extent that of a force dipole aligned with the principal direction of the sprout and with forces at tip and base that point towards each other. Radially pulling forces at the individual sprout tips range (at he displayed time point) from 0.35 nN to 3.48 nN, while forces at the base reached a total of 11.0 nN. Forces at the sprout tips are likely to be the result of actin stress fibers in the tip protrusions that can build up contractile forces when connected to cell-matrix adhesion sites, thereby contributing to movement of the tip cell body [31, 32]. The

origin of the forces at the sprout base and its potential role for cell movement remain elusive, due to the vicinity of the cellular layer that may have contributed substantially to matrix displacements near the sprout base.

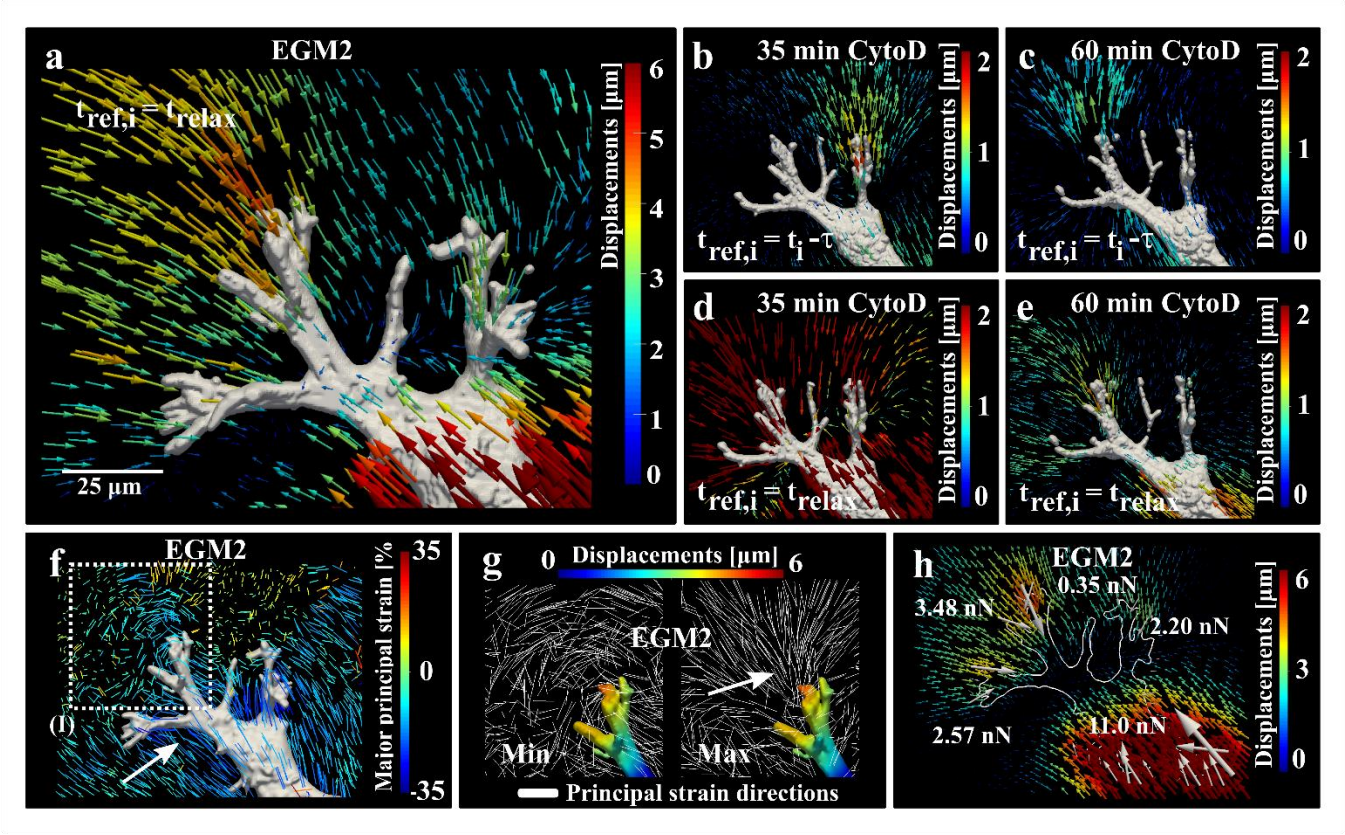


**Fig. 3** Spatial distribution of matrix displacements and strains around a representative angiogenic sprout. **(a)** Absolute displacements, showing a pattern that suggests radially pulling forces at tip protrusions, and oppositely oriented displacements at the sprout base. **(b,c)** Incremental displacements (interval $\tau$ = 5 min) around the sprout in (a) illustrate matrix unloading at the indicated time points during gradual force relaxation (subjected to 500 nM CytoD in (b) and subjected to an additional dose of 4 µM CytoD in (c)), with beads moving away from the sprout. **(d,e)** Absolute displacement field patterns of the same time points in (b) and (c) reveal the reduced pulling activity of the sprout. Displacement arrow lengths in (a-e) are scaled according to the displacement magnitudes. **(f)** Major principal strain distribution shows areas where the matrix is being compressed (negative values) and stretched (positive values). The sprout is highly compressed in the area near the sprout stalk (arrow). The major principal strain at each point is represented by a colored line. Line color and length represent its (signed) magnitude, while its orientation is given by the major principal strain direction. **(g)** Minimum (left) and maximum (right) principal strain directions around the sprout tip indicated in (f-(I)) unveils the orientations in which the matrix near the tip is being compressed ('Min') and stretched ('Max', see arrow). Principal strain direction lines are not scaled to the magnitudes for improved visibility of patterns. Absolute displacement magnitudes at the sprout surface are shown as well (by means of colour map). **(h)** Cellular traction forces (white arrows, scaled by magnitude) calculated from the displacement field based on a nonlinear elastic computational model of the collagen matrix surrounding the sprout. Gradual relaxation was achieved with two doses of CytoD as described in Supplementary Fig. S1. EGM2 = Endothelial Cell Growth Medium-2

The qualitative description of the characteristic displacement field pattern was complemented with a quantitative analysis of absolute displacement fields (**Fig. 4**). To this end, we calculated the principal direction for each individual sprout – called sprout growth direction – and analysed how the absolute matrix displacements change

along this growth direction (see **Fig. 4b**, **Methods** and **Supplementary Fig. S9** for details). Average absolute displacement vectors were calculated as a function of the normalized distance along the growth direction (from sprout base to sprout tip and normalized to the distance between base and sprout) and their magnitude and orientation was plotted. A positive sign was attributed to the magnitude if the average displacement vector pointed towards the tip, a negative sign if it pointed towards the base. The orientation was given by means of the angle with respect to the sprout growth direction (between 0 and 180°; 0°=from base to tip; 180°=from tip to base). This displacement field quantification is first illustrated for a single sprout (and one of its protrusions) during gradual relaxation in Figs. 4a-d. Next, average displacements (n = 20) of sprouts that were relaxed with 4µM CytoD (added after 90 min) are summarized in Figs. 4e-j. Displacement magnitudes were plotted as a function of the normalized distance from base to tip (**Fig. 4d,g,j)**,while displacement angles were summarized in polar histograms (**Fig. 4c,e,f)**.

For the gradually relaxing (representative) sprout the dipole-like displacement pattern is very prominent, with displacement angles that clustered within 30° (at the base) and 150° (at the tip) (**Fig. 4c**, top) and displacement magnitudes that peaked at base and tip, with negative sign at the tip and positive sign at the base (**Fig. 4d**, top). A similar quantitative analysis was performed for a single protrusion of the sprout (region II in **Fig. 4a**). Displacement angles all clustered around 150° (**Fig. 4c**, bottom) and magnitudes were all negative and peaked near the tip of the protrusion (**Fig. 4d**, bottom), suggesting pulling forces exerted by the protrusion.

For the data set of 20 sprouts, average displacement vectors at a given normalized distance at a given time point for a given sprout were further averaged over all sprouts, leading to sprout-averaged displacement vectors as a function of normalized distance and time (**Fig. 4e-j**). When looking at the displacements of these sprouts in EGM2 (0-25 min), the negative peak displacements (-3 µm on average, ranging from -1 to -6 µm) at the sprout tips are again very apparent, confirming the puling activity at the sprout tips. Average displacement vectors at the base display more variability over the 20 sprouts, ranging from -5 to +5 µm and leading to an average value of +1 µm (and thus on average opposite to the displacements at the tip) (**Fig. 4g,h**). Increased variability of displacement vectors at the base might be caused by variability in the organization and mechanical activity of the cellular layer close to the

sprout base. Despite this variability at the base, the radial histograms clearly show that displacements in the vicinity of the sprout closely align to the sprout growth direction, with angles clustering at 30° and 150°.

Interestingly, the dipole-like displacement pattern with oppositely oriented displacement vectors at tips and bases is even more prominent during the force relaxation. Displacements at the base became more positive (red curves in **Fig. 4g**) compared to time points prior to CytoD addition (blue curves in **Fig. 4g**; compare also average values at base between **Fig. 4h** and **i**). Possibly, this has to do with the reduced mechanical activity (and associated variability) of the cellular layer that relaxes first after CytoD addition (as it is closest to the culture medium inlet), therefore interfering less with the dipole-like behaviour of the sprout.

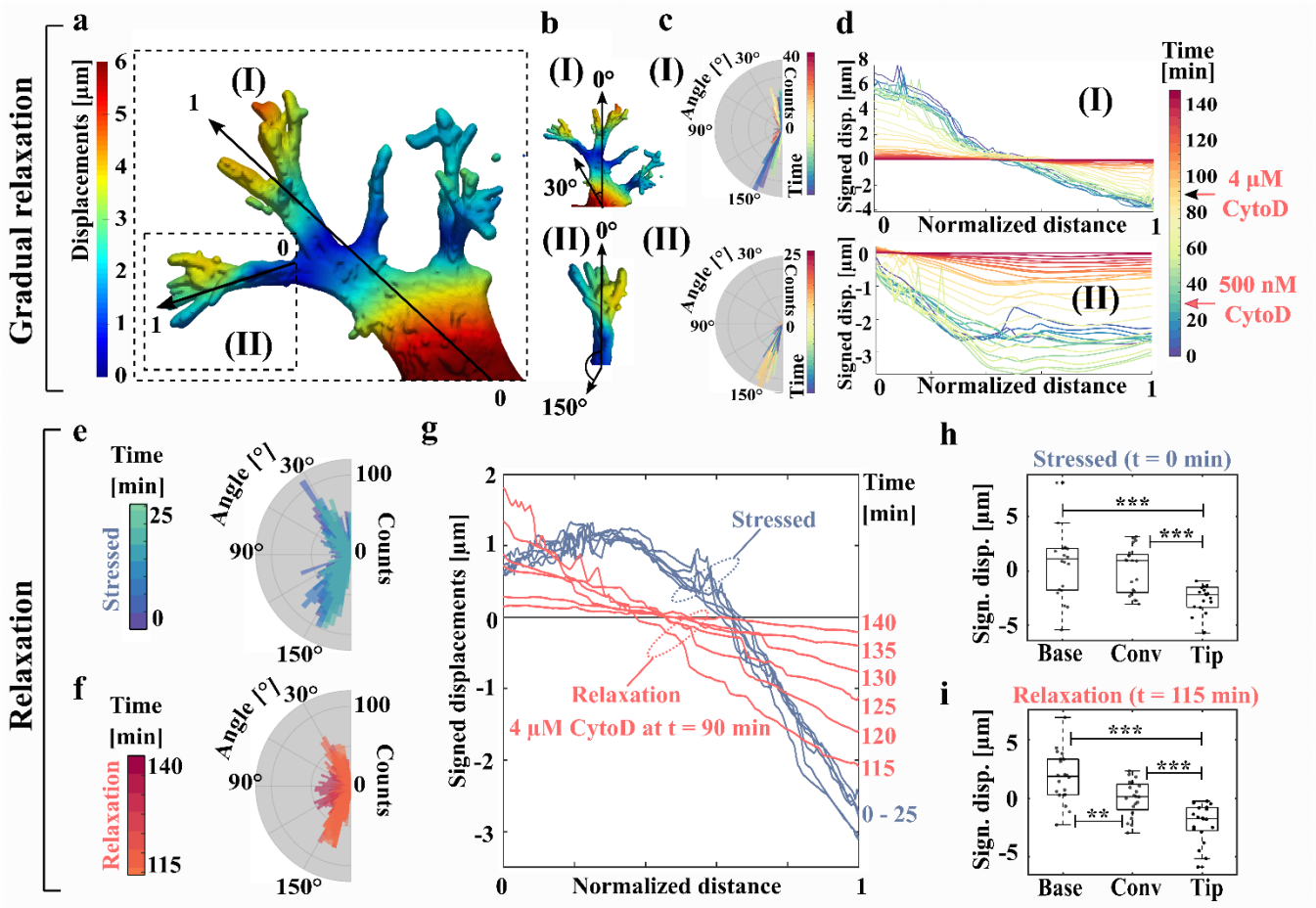


**Fig. 4** Quantitative analysis of absolute displacements with respect to sprout growth direction for one representative sprout during gradual force relaxation with 500 nM CytoD added at t = 30 min (and 4µM CytoD added at t = 90 min to obtain a stress-free state) **(a-d)** and for a data set consisting of 20 sprouts relaxed with 4 µM CytoD (added at t = 90 min) **(e-j)**. **(a)** Selected sprout (same sprout as in Fig. 3), showing absolute displacement magnitudes at the sprout surface and two regions of interest that are further analysed: the entire sprout (I) and a selected protrusion (II). Growth direction (black arrows) for each of the two regions of interest is indicated, together with local coordinate system (0

= base; 1 = tip). **(b)** Same regions of interest as in (a), oriented along their respective growth direction to illustrate their angular coordinate systems for quantifying angles between growth direction and displacement vector. An angle of 0° corresponds to displacement aligned with growth direction (pointing from base to tip), while 180° corresponds to displacement in the opposite direction. Angles of 30° and 150° are shown as examples. **(c)** Radial histograms of displacement angles within the two regions of interest, according to the angular coordinate system displayed in (b). Results are colour-coded for time, corresponding to different time points (0-140 mins) of the displacement microscopy experiment. **(d)** Average signed displacement as a function of the normalized distance to the base (0 = base, 1 = tip see (a)), and as a function of time. Positive and negative signed displacements point towards the tip and the base respectively. **(e,f)** Radial histograms of displacement angles of the average displacement vectors, averaged over 20 sprouts and calculated for time points in EGM2 (e: 0-25 mins) and at the end of the force relaxation (f: 115-140 mins). **(g)** Average signed displacements, averaged over 20 sprouts as a function of the normalized distance to the base for the same time points as in (e). **(h-i)** Boxplots of signed displacement magnitude probed at three positions along the sprout: base (Base), zone of convergence (Conv) (where average displacement = 0 µm) and tip (Tip). Data is shown for the first time point (0 min) and during force relaxation (115 min, i.e. 25 min after initiating the relaxation). Typical average signed displacements in medium ranged between -5 and 5 µm. Significant p-values are indicated with ** for $p < 0.01$ and *** for $p < 0.001$ (see Supplementary Table 2)

Next, we sought to determine whether endothelial sprouts in collagen rely more on pushing or pulling for extending and retracting their protrusions (**Fig. 5**), as previously assessed qualitatively by Du *et al.* [17] in the absence of a stress-free reference state. As pulling forces seem to dominate the mechanical activity of endothelial sprouts (as could be derived from the analysis of absolute displacements in Figs. 3 and 4), we demonstrate that retracting protrusions release (decrease) their pulling forces**,** while sprouts extending their protrusions are building up pulling forces, thereby pulling themselves forward. A total of 10 retracting and 10 extending protrusions (from 20 different sprouts) was imaged over 30 minutes (5 minute scan interval) and a quantitative analysis of displacements with respect to the protrusion growth direction was performed (similar to **Fig. 4**; see **Methods**). In order to better visualize and quantify the total change in matrix displacements that accumulate over consecutive time points of retraction or extension, displacements – further termed cumulative displacements - were calculated with respect to the first time point of the retraction or extension event (see **Methods**). Typical cumulative displacement fields for representative retracting and extending protrusions (and their analysis) are shown in Fig. 5a-g and **Supplementary Video 3 and 4**. In both cases, cumulative displacements become more pronounced with increasing retraction or extension. The matrix in front of the retracting protrusion moves away from the protrusion (**Fig. 5a**; positive sign in **Fig. 5e**; same sign convention as in **Fig. 4**), while for the extending protrusion it moves towards it (**Fig. 5b**; negative sign in **Fig. 5g**). These differences in displacement field directionality between retracting and extending protrusions were further confirmed statistically for the data set of 20 protrusions (10 retracting and 10 extending protrusions), by plotting the average signed cumulative displacement (averaged per sprout and per time point) as a function of protrusion volumetric change (with respect to the first time point; positive (V+) for extension, negative (V-) for retraction) (**Fig. 5h**). Average signed cumulative displacements were significantly different ($p = 0.0044$)

between retracting and extending protrusions and were positive (displacements away from protrusion) for retractions and negative (displacements towards protrusions) for extensions. Finally, average signed absolute displacements around these protrusions were calculated for each time point as well **(Fig. 5j,k)**. Absolute displacements were predominantly negative (towards the protrusion) and were not significantly different between retracting and extending protrusions ($p = 0.2693$), meaning that for both retractions and extensions, pulling instead of pushing forces were dominating in the growth direction. Together with the cumulative displacement data (and its evolution with time), it provides evidence that retracting sprouts tend to release pulling forces, while extending protrusions tend to build up pulling forces, thereby confirming the qualitative assessments reported by Du *et al.* [17].

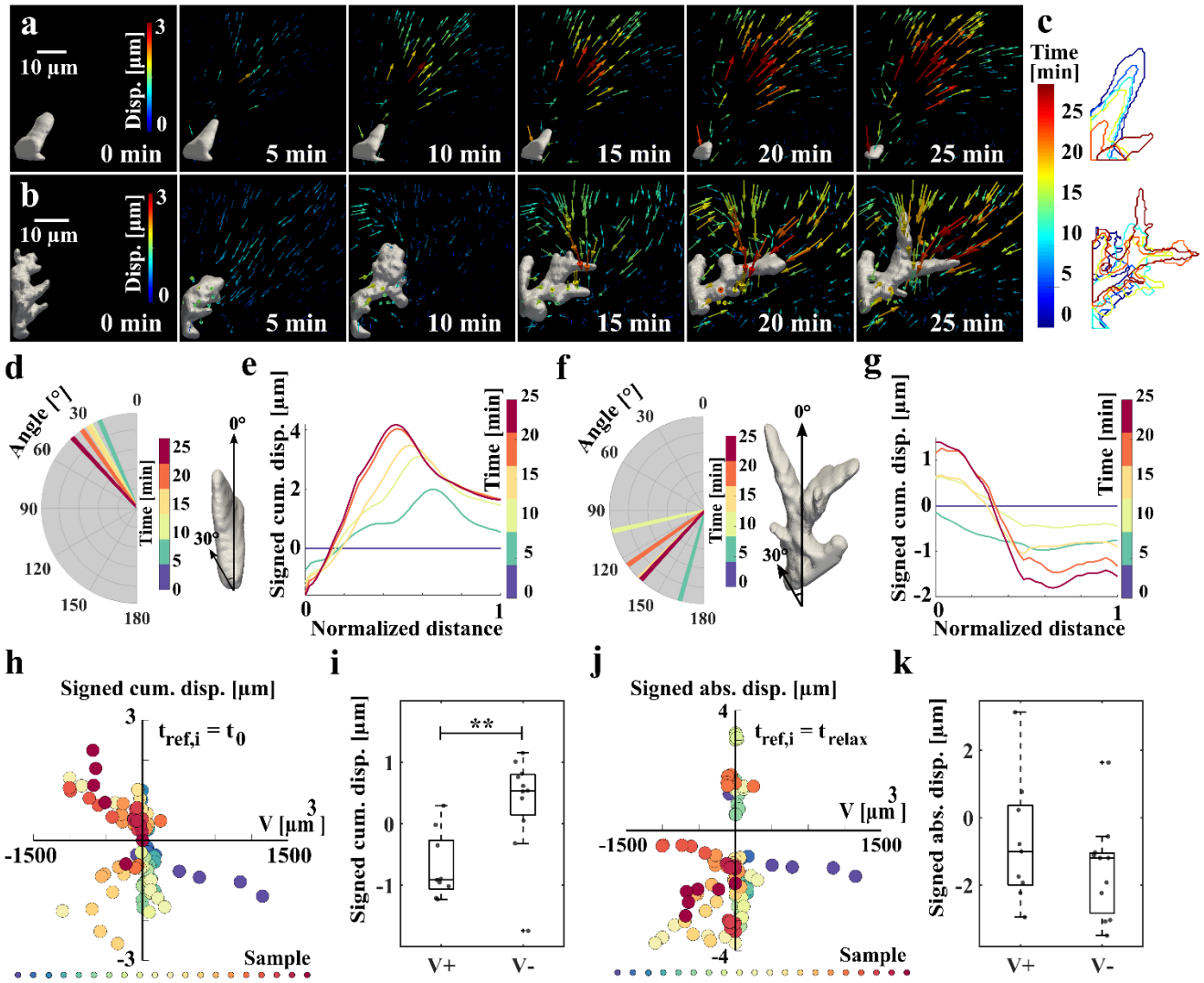

**Fig. 5** Spatio-temporal analysis of displacement fields around retracting and extending sprout protrusions in EGM2. **(a-g)** Analysis for representative sprout protrusions (1 retracting and 1 extending). **(a,b)** Time lapse sequence of displacement fields around a retracting (a) and an extending (b) sprout protrusion. Cumulative displacements are calculated with respect to the first time point. Arrows are scaled to the displacement magnitudes. **(c)** Corresponding changes in protrusion morphology for the same retracting (top) and extending (bottom) protrusion, shown with a contour plot (zt-projection of the protrusion). **(d,f)** Radial histograms showing the average angle of the cumulative displacement vectors for each time point during the retracting (d) and extending (f) event. An angle of 0° corresponds to displacements aligned with protrusion growth direction. An angle of 30° is also shown as an example. **(e,g)** Mean cumulative displacements as a function of time and normalized distance along the protrusion growth direction (0 = protrusion base; 1 = protrusion tip). **(h-k)** Spatio-temporal analysis for a data set consisting of 10 retracting and 10 extending sprout protrusions. **(h,j)** Scatterplot of change of protrusion volume versus mean cumulative (h) and absolute (j) displacements. Data points with the same colour represent consecutive time points from the 30 min time lapse of the same protrusion. **(i,k)** Mean cumulative (h) and absolute (j) displacements, averaged over a set of extending (V+, i.e. volume increase) and retracting (V-, i.e. volume decrease) protrusions. ** indicates $p < 0.01$ (see Supplementary Table 2). Volume changes and displacement values for the consecutive time points in (h) and (j) are averaged per sprout before proceeding with boxplots and significance tests in (i) and (k). All the time points shown in this figure represents data from sprouts in EGM2. To obtain a stress-free reference state, the samples were relaxed with 4 µM CytoD afterwards

In conclusion, we combined a 3D *in vitro* model of endothelial sprouting with 4D displacement microscopy algorithms to retrieve and analyze spatio-temporal displacement fields around endothelial sprouts that result from actin-mediated cytoskeletal forces. From this study, three conclusions can be drawn. Firstly, sprout morphological features such as size and length were demonstrated to be poor predictors of matrix displacement magnitudes. However, sprouts with multiple end protrusions resulted in significantly higher total displacement dynamics than sprouts with a single end protrusion. Regardless of the number of end protrusions, a strong correlation is found between total sprout morphological dynamics and total matrix displacement dynamics, confirming a tight coupling between sprout growth and cell-matrix mechanical activity as reported previously in the field [18, 19]. This data is coherent with the fan-like pattern of collagen fibrils previously reported near the sprout tip by Kirkpatrick *et al.* [28]. While Yoon et al. observe maximal pulling at sprout tips [16], the present study extends the analysis of the phenomenon by spatio-temporally quantifying the relation between displacement metrics and morphometrics. Secondly, a recurrent displacement field pattern was found over different sprout morphologies, with displacement maxima near sprout tip and base that suggest force dipole-like sprout behaviour with radially pulling forces at the sprout tips. Finally, the analysis of local displacement fields around retracting and extending sprout protrusions confirmed the predominant role of pulling instead of pushing forces: while retracting protrusions were found to mainly reduce their pulling forces and therefore release the collagen matrix, extending protrusions increased their pulling forces and pulled themselves forward. While similar bead movement patterns have been observed by Du *et al.* [17], the stress-free reference state and spatio-temporal analysis of a sufficiently large dataset conducted in this

study were crucial for a mechanically sound interpretation of the observed displacement patterns. This is demonstrated by showing incremental displacements that resemble push-like behavior (beads moving away from the sprout) but appear to be nevertheless pulling when compared to a stress-free state (beads appear even further away from the sprout in the relaxed state). Overall, our study demonstrates a key role of cell-matrix mechanics in sprouting angiogenesis, and contributes to deciphering how *in vitro* endothelial sprouts mechanically interact with their micro-environment.

## REFERENCES


1. Carmeliet P (2003) Angiogenesis in health and disease. Nat Med 9:653–660. https://doi.org/10.1038/nm0603-653
2. Kniazeva E, Putnam AJ (2009) Endothelial cell traction and ECM density influence both capillary morphogenesis and maintenance in 3-D. Am J Physiol - Cell Physiol 297:C179–C187. https://doi.org/10.1152/ajpcell.00018.2009
3. Elliott H, Fischer RS, Myers KA, et al (2015) Myosin II controls cellular branching morphogenesis and migration in three dimensions by minimizing cell-surface curvature. Nat Cell Biol 17:137–147. https://doi.org/10.1038/ncb3092
4. Gerhardt H (2008) VEGF and endothelial guidance in angiogenic sprouting. Organogenesis 4:241–246
5. Geudens I, Gerhardt H (2011) Coordinating cell behaviour during blood vessel formation. Development 138:4569–4583. https://doi.org/10.1242/dev.062323
6. Travasso RDM (2011) The Mechanics of Blood Vessel Growth. In: Vasculogenesis and Angiogenesis - from Embryonic Development to Regenerative Medicine. InTechOpen, Rijeka, Rijeka Croatia, pp 187–204
7. Santos-Oliveira P, Correia A, Rodrigues T, et al (2015) The Force at the Tip - Modelling Tension and Proliferation in Sprouting Angiogenesis. PLOS Comput Biol 11:1–20. https://doi.org/10.1371/journal.pcbi.1004436
8. De Smet F, Segura I, De Bock K, et al (2009) Mechanisms of vessel branching: filopodia on endothelial tip cells lead the way. Arterioscler Thromb Vasc Biol 29:639–649. https://doi.org/10.1161/ATVBAHA.109.185165
9. Schmidt M, Paes K, De Mazière A, et al (2007) EGFL7 regulates the collective migration of endothelial cells by restricting their spatial distribution. Development 134:2913–2923. https://doi.org/10.1242/dev.002576
10. Sauteur L, Krudewig A, Herwig L, et al (2014) Cdh5/VE-cadherin Promotes Endothelial Cell Interface Elongation via Cortical Actin Polymerization during Angiogenic Sprouting. Cell Rep 9:504–513. https://doi.org/10.1016/j.celrep.2014.09.024
11. Kraning-Rush CM, Califano JP, Reinhart-King CA (2012) Cellular Traction Stresses Increase with Increasing Metastatic Potential. PLoS One 7:e32572. https://doi.org/10.1371/journal.pone.0032572
12. Califano JP, Reinhart-King CA (2009) The Effects of Substrate Elasticity on Endothelial Cell Network Formation and Traction

Force Generation. In: Soc MB (ed) 31st Annual International Conference of the IEEE Engineering. Minneapolis, pp 3343–3345

13. Reinhart-King CA, Dembo M, Hammer DA (2005) The Dynamics and Mechanics of Endothelial Cell Spreading. Biophys J 89:676–689. https://doi.org/10.1529/biophysj.104.054320

14. Stout DA, Bar-Kochba E, Estrada JB, et al (2016) Mean deformation metrics for quantifying 3D cell–matrix interactions without requiring information about matrix material properties. Proc Natl Acad Sci 113:2898–2903. https://doi.org/10.1073/pnas.1510935113

15. Mabeta P, Pepper MS (2009) A comparative study on the anti-angiogenic effects of DNA-damaging and cytoskeletal-disrupting agents. Angiogenesis 12:81–90. https://doi.org/10.1007/s10456-009-9134-8

16. Yoon C, Choi C, Stapleton S, et al (2019) Myosin IIA–mediated forces regulate multicellular integrity during vascular sprouting. Mol Biol Cell 30:1974–1984. https://doi.org/10.1091/mbc.e19-02-0076

17. Du Y, Herath SCB, Wang Q-GG, et al (2016) Three-Dimensional Characterization of Mechanical Interactions between Endothelial Cells and Extracellular Matrix during Angiogenic Sprouting. Sci Rep 6:1–14. https://doi.org/10.1038/srep21362

18. Kniazeva E, Weidling JW, Singh R, et al (2012) Quantification of local matrix deformations and mechanical properties during capillary morphogenesis in 3D. Integr Biol 4:431–439. https://doi.org/10.1039/c2ib00120a

19. Du Y, Herath SCB, Wang Q-G, et al (2012) Endothelial-cell-mediated Displacement of Extracellular Matrix during Angiogenesis. World Acad Sci Eng Technol 72:1541–1546

20. Steinwachs J, Metzner C, Skodzek K, et al (2016) Three-dimensional force microscopy of cells in biopolymer networks. Nat Methods 13:171–176. https://doi.org/10.1038/nmeth.3685

21. Owen LM, Adhikari AS, Patel M, et al (2017) A cytoskeletal clutch mediates cellular force transmission in a soft, three-dimensional extracellular matrix. Mol Biol Cell 28:1959–1974. https://doi.org/10.1091/mbc.E17-02-0102

22. Koch TM, Münster S, Bonakdar N, et al (2012) 3D Traction Forces in Cancer Cell Invasion. PLoS One 7:e33467. https://doi.org/10.1371/Citation

23. Kim J, Jones CAR, Groves NS, Sun B (2016) Three-Dimensional Reflectance Traction Microscopy. PLoS One 11:1–17. https://doi.org/10.1371/journal.pone.0156797

24. Jorge-Peñas A, Bové H, Sanen K, et al (2017) 3D full-field quantification of cell-induced large deformations in fibrillar biomaterials by combining non-rigid image registration with label-free second harmonic generation. Biomaterials 136:86–97. https://doi.org/10.1016/j.biomaterials.2017.05.015

25. Condor M, Steinwachs J, Mark C, et al (2017) Traction Force Microscopy in 3-Dimensional Extracellular Matrix. Curr Protoc Cell Biol 75:1–20. https://doi.org/10.1002/cpcb.24

26. Malandrino A, Trepat X, Kamm RD, Mak M (2019) Dynamic filopodial forces induce accumulation, damage, and plastic remodeling of 3D extracellular matrices. PLoS Comput Biol 15:1–26. https://doi.org/https://doi.org/10.1371/journal. pcbi.1006684

27. Kim J, Feng J, Jones CAR, et al (2017) Stress-induced plasticity of dynamic collagen networks. Nat Commun 8:1–7. https://doi.org/10.1038/s41467-017-01011-7

28. Kirkpatrick ND, Andreou S, Hoying JB, Utzinger U (2007) Live imaging of collagen remodeling during angiogenesis. Am J Physiol Heart Circ Physiol 292:H3198–H3206. https://doi.org/10.1152/ajpheart.01234.2006

29. Legant WR, Miller JS, Blakely BL, et al (2010) Measurement of mechanical tractions exerted by cells within three-dimensional matrices. Nat Methods 7:969–971. https://doi.org/10.1038/nmeth.1531.Measurement

30. Bayless KJ, Kwak H-I, Su S-C (2009) Investigating endothelial invasion and sprouting behavior in three-dimensional collagen matrices. Nat Protoc 4:1888–1898. https://doi.org/10.1038/nprot.2009.221

31. Martins GG, Kolega J (2006) Endothelial Cell Protrusion and Migration in Three-Dimensional Collagen Matrices. Cell Motil Cytoskeleton 63:101–115. https://doi.org/10.1002/cm.20104

32. Doyle AD, Carvajal N, Jin A, et al (2015) Local 3D matrix microenvironment regulates cell migration through spatiotemporal dynamics of contractility-dependent adhesions. Nat Commun 6:8720. https://doi.org/10.1038/ncomms9720

## METHODS

Methods and any associated references are specified within the Supplementary Information available in the online version of the paper.

## AUTHOR CONTRIBUTIONS

H.V.O., M.M.V. and A.J.P. devised the overall experimental strategy. H.V.O. and P.C. provided the cell culture facilities. M.R. provided the microscopy facilities. M.M.V. extended the *in vitro* model for 4D displacement microscopy. C.S. operated and extended the microscopy setup for live cell imaging. M.M.V. and C.S. performed the sprouting experiments, diffusion experiments and acellular control experiments. A.P.J. and J.B.F. developed all computational algorithms for displacement and morphology quantification. M.M.V. and A.J.P. pre-processed the data. J.B.F. and M.M.V. developed code for statistical analysing. M.M.V. analysed the data, composed the main figures and rendered all videos. J.B.F. developed computational algorithms for strain calculations and composed the figures related to strains. T.H. developed the computational model of collagen mechanics and calculated sprout forces. M.M.V., A.J.P., J.B.F. and H.V.O. discussed and interpreted the data. The manuscript and figure design was prepared by M.M.V. and was finalised with input from all authors.

## COMPETING FINANCIAL INTERESTS

The authors declare no competing financial interests.

## DATA AND CODE AVAILABILITY

The data and code that support the findings of this study are available within the Supplementary Figures, Table, Videos, cited references or from the corresponding author upon request. The analytical code (together with a sample dataset and guidelines) and laboratory protocols are available on the website of the corresponding author: https://www.mech.kuleuven.be/en/bme/research/mechbio, by navigating to the Software and Protocols section.